In-situ experimental benchmarking of solid oxide fuel cell metal interconnect solutions

Bianco, Manuel; Caliandro, Priscilla; Diethelm, Stefan; Yang, Shicai; Dellai, Alessandro; Van herle, Jan; Steinberger-Wilckens, Robert

DOI:
10.1016/j.jpowsour.2020.228163

Document Version
Publisher's PDF, also known as Version of record

Citation for published version (Harvard):
Bianco, M, Caliandro, P, Diethelm, S, Yang, S, Dellai, A, Van herle, J & Steinberger-Wilckens, R 2020, 'In-situ experimental benchmarking of solid oxide fuel cell metal interconnect solutions', *Journal of Power Sources*, vol. 461, 228163. https://doi.org/10.1016/j.jpowsour.2020.228163

Journal of Power Sources 461 (2020) 228163

Contents lists available at ScienceDirect

Journal of Power Sources

journal homepage: www.elsevier.com/locate/jpowsour

In-situ experimental benchmarking of solid oxide fuel cell metal interconnect solutions

Manuel Bianco [a,*], Priscilla Caliandro [a], Stefan Diethelm [b], Shicai Yang [c], Alessandro Dellai [d], Jan Van herle [a], Robert Steinberger-Wilckens [e]

[a] GEM Group, Inst. Mech. Eng., EPFL Valais, CH-1951, Sion, Switzerland
[b] SOLIDpower sa, Yverdon le Bains, Switzerland
[c] Teer Coatings Ltd., West Stone House, West Stone, Berry Hill Industrial Estate, Droitwich, WR9 9AS, UK
[d] SOLIDpower spa, Mezzolombardo, Italy
[e] Centre for Fuel Cell and Hydrogen Research, School of Chemical Engineering, University of Birmingham, Edgbaston, Birmingham, B15 2TT, UK

HIGHLIGHTS

- 3 SOFC 6-cell stacks are run for 10 000 h each and post-test characterized.
- AISI441/K41 can operate as interconnect on long periods.
- Commercial SRUs containing WPS coated interconnect are reliable on the long period.
- SRUs containing PVD coated interconnect gave the lowest voltage degradation values.

ARTICLE INFO

Keywords:
Coatings
Degradation
Post-test analysis
SOFC stacks
Spinel
Stainless steels

ABSTRACT

The progress in the diffusion of solid oxide fuel cell (SOFC) as commercial devices is not paired by literature production. Articles describing the behaviour of SOFC stacks are rare because of confidentiality reasons for commercial suppliers while research centres prefer to focus on single components or low technology readiness level research.

This article aim to fill this gap presenting the analysis of three short stacks run in operative conditions for 10 000 h each. The stacks are characterized through voltage vs time curves, electron microscopy, and electrochemical impedance spectroscopy. Focus is given on the interconnect; notably on the different types of coatings, varying for composition ($MnCo_2O_4$, $MnCo_{1.8}Fe_{0.2}O_4$) and deposition technique (atmospheric plasma spray-APS, physical vapour deposition-PVD, wet powder spraying-WPS). Nitriding of the steel substrate as a solution to improve the chromium retention properties is tested as well.

Results: indicate that coating deposition technique is the most important parameter, with single repeat unit (SRU) containing PVD coating showing the lowest voltage degradation rate. Commercial ferritic stainless steel K41 confirmed to be a reliable choice if coupled with a coating. Moreover, SRU containing WPS coating demonstrated to be more reliable than expected from standard area specific resistance 4-probe test.

1. Introduction

A solid oxide fuel cell (SOFC) stack in a stationary application is expected to operate for at least 40 000 h in order to match the specifications for conventional heating, combined heat and power, and power generation equipment [1–3]. This requires a set of materials able to withstand high temperature (600–900 °C) and a demanding environment with high temperatures and partially high humidity for several tens of thousands of hours [4–7].

Assessing the materials properties over such a span of time brings a substantial investment in equipment and working hours. Due to this high effort, is it a preferred practice to test single components (cells [8–11], interconnects, sealing [12–14], etc.) separately on a smaller scale and for shorter periods. Accelerated testing methods, that would solve this problem, have been much discussed but not successfully implemented yet [15–17]. The representativeness of single component

* Corresponding author.
E-mail address: manuel.bianco.pro@gmail.com (M. Bianco).

https://doi.org/10.1016/j.jpowsour.2020.228163
Received 21 January 2020; Received in revised form 3 April 2020; Accepted 6 April 2020
Available online 17 April 2020

testing for evaluating real applications is however partial, since the multiple interactions between the single components are ignored in such assessment. Only long-term SOFC stack testing can deliver real insight into the lifetime and robustness of the technology.

The interconnect component in SOFC stacks is especially critical [18]. Its material has to be electrically highly conductive, gastight, mechanically stable at high temperatures, stable in oxidising and reducing atmospheres, including high humidity, as well as in dual atmospheres (one side reducing, the other oxidising). At the same time it has to be cheap and easy to shape. Today, ferritic stainless steels are the most employed interconnect material. They supply most of the aforementioned properties, although releasing volatile chromium species when presented with humid air [19]. This chromium hydroxide will interact with cathode materials of SOFC to form spinels [20–22] or deposit as chromium oxide, in both cases reducing the activity of the cathode [23–25].

In order to prevent this from happening, or at least reduce the effect, protective coatings are applied to SOFC interconnects [26–28]. The EU project SCORED 2:0 (contract no. 325331, 'Steel Coatings for Reducing Degradation in SOFC', 2014 to 2017) compared different ways of applying coatings on different steel qualities. Wet Powder Spraying (WPS), Inkjet Printing, Atmospheric Plasma Spraying (APS), Atomic Layer Deposition (ALD), Surface Modification, and Physical Vapour Deposition (PVD) were the methods assessed on Sandvik HT, CroFer 22H, and AISI 441/K41 steels. The comparative study of SOFC interconnect materials and coatings has been previously published [29]. These results were obtained with a modified 4-probe testing method, which used 1 cm^2 contact area samples [30,31]. The results were organised by ranking the area specific resistance (ASR) and the chromium retention property of each tested sample. The conclusions indicated that dense coatings, such as those deposited via atmospheric plasma spraying and physical vapour deposition, offer the best performing solutions. In addition, the study suggested that, in presence of a coating, stainless steel Crofer 22H [32] did not outperform the cheaper commercial grade AISI441/K41 [33], at least not under the conditions and the span of time tested.

However, the modified 4-probe testing method does not exactly represent the materials setting inside an SOFC stack. The contact surface is restricted to 1 cm^2, the gases do not freely flow between the samples, the samples are not in contact with a complete cell, and the testing period is short compared to the desired SOFC device lifetime (1000 h vs. 40 000 h).

The results obtained with the small samples therefore needed to be validated in an SOFC stack. The best combinations resulting from the small samples, together with a standard commercial solution (K41 steel substrate coated through wet powder spray), were transferred onto commercially fabricated interconnects and tested in three 6-cell short-stacks for 10 000 h.

Among the initial conclusions drawn in the preceding study [29], the present article aims to assess whether:

- there is a correspondence in the ASR and Cr retention results between those small samples and the industrial size metal interconnects tested in a real stack environment;
- steel nitriding helps to reduce Cr evaporation also in real stack operating conditions;
- K41 steel is a reliable alternative to higher Cr containing alloys, such as Crofer 22H.

This article presents the results obtained from the tested short-stacks. i-V curves, impedance spectroscopy and SEM/EDS cross sections were used in the characterisation.

The literature on post-test or post-operational analysis of SOFC stacks is scarce, partly because SOFC suppliers refrain from disclosing information related to interconnect geometry. As a result, the few published studies on metal interconnects (MICs) operated in stacks mainly come from research centres. For example, Forschungszentrum Jülich has published results from post-test characterisation of stacks tested up to 35 000 h and containing atmospheric plasma spray (APS) (densly) coated Crofer 22H interconnects or wet powder spray (WPS) (porous) coated Crofer 22 APU [34–38]. Their analyses confirmed the good adhesion of the coatings to the steel substrates and the presence of a mild degradation process in case of dense APS coating, while the WPS coating presented poorer performances. A dense coating would generally be expected to improve chromium retention properties.

A few other sources are found in literature [39], but most of the solutions tested on small samples remain unexplored or not reported for long-term operation or under SOFC stack conditions. In addition, the excellent corrosion resistance at high temperature of Crofer 22 APU or H is counterbalanced by the high cost of these steel grades; one of the aims of this paper is to gather more information about the long-term reliability of the cheaper commercial grade steel AISI441/K41 [40–42].

In this study, 6 combinations of AISI441/K41 interconnects with different types of coating composition, deposition methods, and surface treatment (nitriding [29]) were compared with a manganese cobalt oxide (MCO), wet powder spray (WPS) treated reference.

2. Materials and experiments

Three stacks containing 6 single repeating units (SRUs) were each tested for about 10 000 h, each SRU containing one cell and one metal interconnect. The cell (supplied by SOLIDpower S.p.a.) was identical for all the stacks, it is an anode supported cell with standard Ni-YSZ anode, on which an electrolyte (YSZ), a barrier layer (GDC), LSCF:GDC composite cathode, LSCF, and current collector layer are deposited and sintered. The cells are produced by anode and electrolyte co-casting and co-sintering followed by screen-printing of the cathode layers. The cell layers' thicknesses are 240 μm for the anode support, 10 μm for the thin electrolyte, 6–8 μm for the barrier layer, and 60 μm for the bilayer cathode, respectively. Whereas the coated metallic interconnects (MICs) varied in pairs, as described in Table 1.

The MCO base coating composition was a spinel of manganese and cobalt with the stoichiometric formula $MnCo_2O_4$. The Fe-doped formula $MnCo_{1.8}Fe_{0.2}O_4$ (MFC) was also tested. Three coating deposition techniques were applied: atmospheric plasma spraying (APS) by Turbocoating S.p.a., physical vapour deposition (PVD) by Teer Coatings Ltd, and wet powder spraying (WPS) by SOLIDpower S.p.a. The choice of these coatings derived from the results obtained on small coupons [29]. The same article provides details on the coating processes. The main parameters of these coatings are repeated here: for WPS ones the coating as deposited is open porous and 10–30 μms thick; APS and PVD coatings are dense with thicknesses of ca. 50–60 μms and 10–30 μms respectively. MCF was the coating with the lowest average contact resistance (5–10 mOhm*cm^2); APS and PVD were chosen because of the Cr retention and electrical contact properties, and finally a nitrided steel substrate was added to the comparison to validate its chromium-blocking properties. WPS is the technique with lowest manufacturing cost among those

Table 1
MIC coating compositions, coating deposition techniques and application of a nitriding pre-process. MCO = $MnCo_2O_4$; MCF = $MnCo_{1.8}Fe0.2O_4$; APS = Atmospheric Plasma Spraying; WPS = Wet Powder Spraying.

	Steel substrate	Nitriding	Coating	Deposition tech.
STACK A	K41	NO	MCF	WPS
STACK A	K41	YES	MCO	WPS
STACK A	K41	NO	MCO	WPS
STACK B	K41	NO	MCF	APS
STACK B	K41	YES	MCO	APS
STACK B	K41	NO	MCO	WPS
STACK C	K41	NO	MCF	PVD
STACK C	K41	NO	MCO	PVD
STACK C	K41	NO	MCO	WPS

presented here.

SOLIDpower S.p.a. assembled all the stacks and the MICs according to their standard stack geometry.

Each SRU type was applied twice in order to obtain statistically more meaningful results. The bottom and top SRUs in all stacks were those treated with WPS MCO, to be used as a baseline (3rd line for each stack A, B, C in Table 1).

The short stacks were tested in three different research sites (EPFL, ENEA, SOLIDpower S.p.a) under the same operating conditions: air on the cathode side, N_2/H_2 (40/60 %vol.) on the anode side, average temperature of 750 °C, and a current density of 0.41 Acm^{-2}. After completion of the tests, each stack was cooled under forming gas (5% H_2 in N_2), and removed from the test bench while maintaining stack compression. Subsequently, epoxy resin (Struers Epofix kit) was used to embed the entire short stack. Vacuum was applied to help the resin penetrating the pores of the porous ceramics.

After the resin solidification, the stack was cut into smaller pieces of about 5*5*5 cm^3 and then polished with SiC papers following a grit size sequence of: 320, 600, 1200, 2500, 4000 and finished with diamond paste of 6, 3 and 1 μm on felt discs. The polished surfaces were finally carbon coated to avoid charge accumulation during SEM observations.

The cross sections for stacks A and B were taken in the middle of the stack, while stack C underwent a more detailed microstructural analysis with cuts at the inlet and the outlet. In all cases, the cuts were done perpendicular to the flow directions.

The cross sections were observed with an FEI TENEO SEM coupled with a Bruker EDX detector. The typical SEM acceleration voltage was between 15 and 30 kV. Subsequently, The obtained images were treated with a semiautomatic routine. Imaging software Adobe Photoshop and Fiji were used to segment oxide layer. A Matlab routine calculated the average thickness out of six different region of interests.

3. Results

Voltage degradation of each stack is presented in Fig. 1. The stacks have been labelled A, B, and C as in Table 1.

The voltage evolution over time for stack A presents multiple interruptions, due to unwanted power cuts. Since the degradation value of each SRU is extrapolated from the V(t) curve, the degradation values for Stack A are not considered in the discussion. However, this stack is still analysed by SEM/EDS to assess the chromium retention properties related to the steel nitriding process. These observations are still relevant since chromium diffusion from the steel substrate is assumed to be purely temperature-controlled [43], with no influence of conditions of electrochemical operation.

Stack B and C underwent controlled shutdowns, with the peaks in the graphs resulting from i-V measurements taken at regular time intervals. In a few cases the short stack C was set in stand-by at OCV for laboratory maintenance reasons.

The SRUs containing the same type of metal interconnect and coating are represented with the same colour.

Table 2 reports the degradation rate for each SRU of stacks B and C. The SRUs are listed according to their position in the short stack (1–6), with the first and last lines being the bottom and top SRUs in the test furnace, respectively. Even if SRUs are labelled according to the type of the deposited coating (e.g. WPS MCO), the losses also include the contribution of the cell. This nomenclature will be retained hereafter.

The degradation rate of the SRUs (Table 2) is calculated taking the value at 1000 h as starting reference and the last recorded point as final one. The first 1000 h are not considered, in order to exclude the influence of transient phenomena taking place in the cell and in the interconnect at the beginning of stack operation.

Less than 0.5%kh^{-1} of voltage degradation is the target value for a stack lifetime of 40 000 h, and below 0.25%kh^{-1} for continuous operation over 10 years. In this sense, all tested SRUs in stacks C fulfil the requirements. The SRUs with WPS coatings show similar average degradation rates in the short stack B, while in short stack C, the values differ significantly. The WPS MCO #2 in STACK C and APS MCF #1 in Fig. 1 appear to differ from the others in behaviour. It is worth noting that WPS MCO #2 voltage curves suffer relevant drops at around 7200, 8000 and 9200 h, and the overall degradation value hides this behaviour. The low number of samples might have an impact on the results shown in Fig. 1 and Table 2. Nevertheless, some indicative results can be drawn from the tests.

The WPS MCO SRUs (baseline case) show the highest average degradation rates. On average, these are followed by APS SRUs, with PVD layer containing SRUs generally showing the lowest degradation rates. This ranking agrees with the results obtained from small samples [29], though the degradation of APS MCF #1 was unexpectedly high. On the other hand, the degradation rates of SRUs containing nitrided steel substrates (APC MCO) were lower than expected from the area specific resistance (ASR) tests on small samples.

Moreover, the comparison of the SRUs degradation rates shows a bigger gap between APS and PVD coated MICs than expected from small sample results [29]. APS and PVD technologies were expected to produce MICs with a rather similar degradation rate.

Looking at the absolute voltage values after 10 000 h of operation instead (Fig. 1), the difference between the PVD and the APS containing SRUs were less relevant. The best voltage values are obtained for the SRUs with PVD applied coatings MCO#1 and MCF#2 at 0.775 V, with good coincidence of both level voltages and a very low degradation rate. For SRUs with APS protective layers the best performance is N + MCO#1 with 0.75 V and finally 0.72 V were the highest value at 10 000 h for the WPS MCO group. The Fe doping in the PVD coatings did not lead to a noticeable improvement.

Steel nitriding in the case of APS containing SRUs seems to help stabilizing the degradation process.

The V(t) curves are a way of monitoring the global SRU performance. It is of equal interest to discriminate the cell and interconnect contributions to the total ohmic losses.

Therefore, the three stacks are embedded in epoxy resin, cross-cut and the cross-section surfaces analysed by SEM/EDS. The microscopy and chemical analyses supplied information about the status of the cell and of the interaction between the interconnects and the other SRU components. Stack A and B will be discussed together in the following, while stack C will be treated separately.

3.1. SEM/EDS observations

Fig. 2 provides SEM/EDS observations for WPS-deposited MCO on regular and nitrided K41 substrates, as well as for APS-deposited MCF on standard K41 substrate. These repeat elements stem from stacks A and B. The EDS element maps are reported for chromium, cobalt, iron and manganese.

The APS coatings maintained the as deposited composition: the EDS analysis found no iron in the MCO and no excess of iron in the MCF. The steel corrosion below the coating consists of Cr_2O_3 and likely $(CrMn)_3O_4$. The latter spinel presence cannot be fully confirmed due to the overlap with the signal coming from Mn contained in the coating. Discontinuous layer of SiO_2 is present at the chromia/steel interface. The diffusion barrier action is effective, no chromium is detected in any of the APS SRUs cathode contacting material and, at the same time, no third elements are detected in the coatings. The oxide scale grown on nitrided substrates has a homogenous morphology, whereas on non-nitrided substrate the scale profile is more irregular. The thick and dense APS spinel coatings hinder the oxygen migration towards the stainless steel [28], therefore the oxide layer is thin: an average 4.6 μm for non-nitrided versus 2.7 μm for nitrided ones. As observed also in small ASR tested samples [29], the presence of such a thick and dense coating (APS) masks the effect of the nitriding process on the Cr retention property.

In contrast, the behaviour of WPS porous coatings on standard

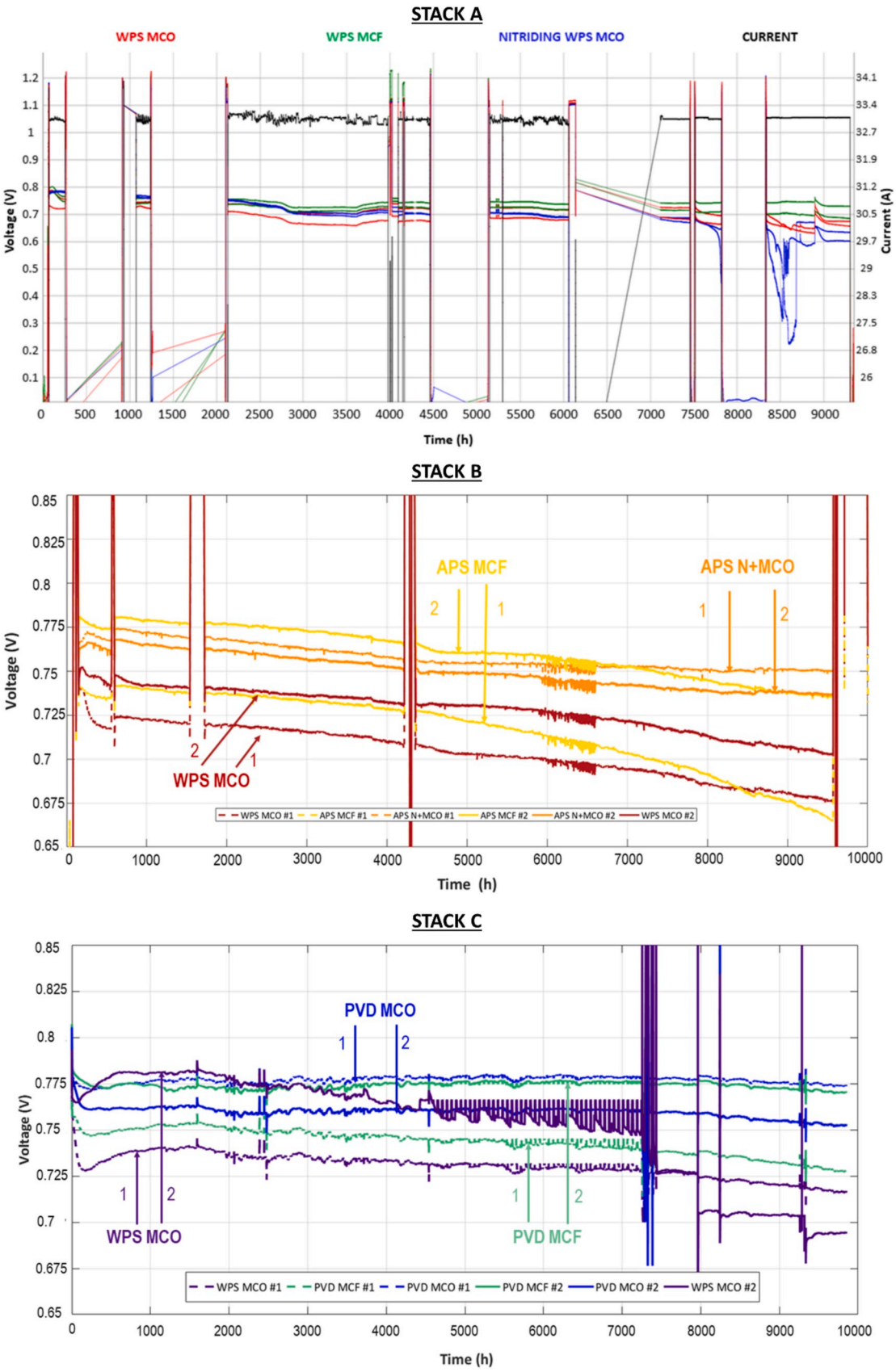

Fig. 1. Voltage over time of 6-cell SOFC short stacks tested at different sites. Multiple interruptions damaged the cells in stack A. Stack B was tested by an industrial partner, Stack C was tested at EPFL. The testing protocol was the same for all stacks.

Table 2
Degradation rates for stacks B and C. Degradation rates is calculated between 1000 and 10 000 h of operation. Stack planes are listed from bottom to top.

STACK B ('APS' vs baseline)			STACK C ('PVD' vs baseline)		
MIC	Degrad. (%kh^{-1})	Degrad. (μV/h)	MIC	Degrad.(%kh^{-1})	Degrad. (μV/h)
WPS MCO #1	0.72	23.14	WPS MCO #1	0.38	12.49
APS MCF #1	1.14	37.5	PVD MCO #1	0.40	13.37
APS N + MCO #1	0.34	11.67	PVD MCF #1	0.042	1.45
APS MCF #2	0.64	22.05	PVD MCO #2	0.059	2.03
APS N + MCO #2	0.45	15.31	PVD MCF #2	0.15	5.08
WPS MCO #2	0.67	22.10	WPS MCO #2	1.35	46.85

stainless steel is the sum of several interactions. Strontium, iron, and chromium ions diffused across the metal/coating/perovskite interfaces. The WPS SRUs containing iron-doped coating (MCF) have a corrosion behaviour coherent with the SRUs containing MICs coated with pure manganese cobalt spinel, both in terms of scale thickness and morphology. For the nitrided interconnects coated with porous WPS MCO instead, the reactivity at the MIC/coating/perovskite interface is reduced. The average oxide layer thickness can be considered as a parameter indicative of the corrosion kinetics: 11 μm for the standard MICs with WPS MCO, 7 μm on nitrided MIC with WPS MCO. The standard deviation in the value of the scale thickness for the nitrided substrates is smaller than for the regular substrate (1.05 μm vs 5.3 μm). The inward corrosion front in the nitrided MICs was homogeneous all along the interface despite the presence of outward iron oxidation. In non-nitrided steel substrates instead, there are isolated spots with aggravated corrosion, these regions present pits entering the steel substrate. The presence of an external iron oxidation has some similarities with the iron breakaway corrosion phenomenon [44]. The Fe distribution suggests a failure of the passivation layer during the first stages of corrosion, so that iron oxidation in nitrided MICs affected the whole interconnect/coating/perovskite interface until the chromia passivation layer was established. In turn, this observed Fe oxidation suggests that nitrogen acts as a scavenger element for chromium in the first phase of the corrosion process [45].

In the surface-nitrided steel substrates, no chromium is found in the contacting perovskite. The nitrogen activity towards chromium therefore improves the chromium barrier properties of the WPS deposited coating and the stabilisation of the corrosion process.

Referring to the performances in STACK B, the SRUs containing surface-nitrided MICs have lower degradation rates in the long-term. STACK A gives an opposite indication, but as explained before, these stack data are less reliable.

Two cross-sections were extracted from stack C and analysed by SEM/EDS. To better assess the degradation, one sample was cut at the inlet and a second one at the outlet of the stack (Fig. 3).

The tests previously performed on small ASR samples indicated that

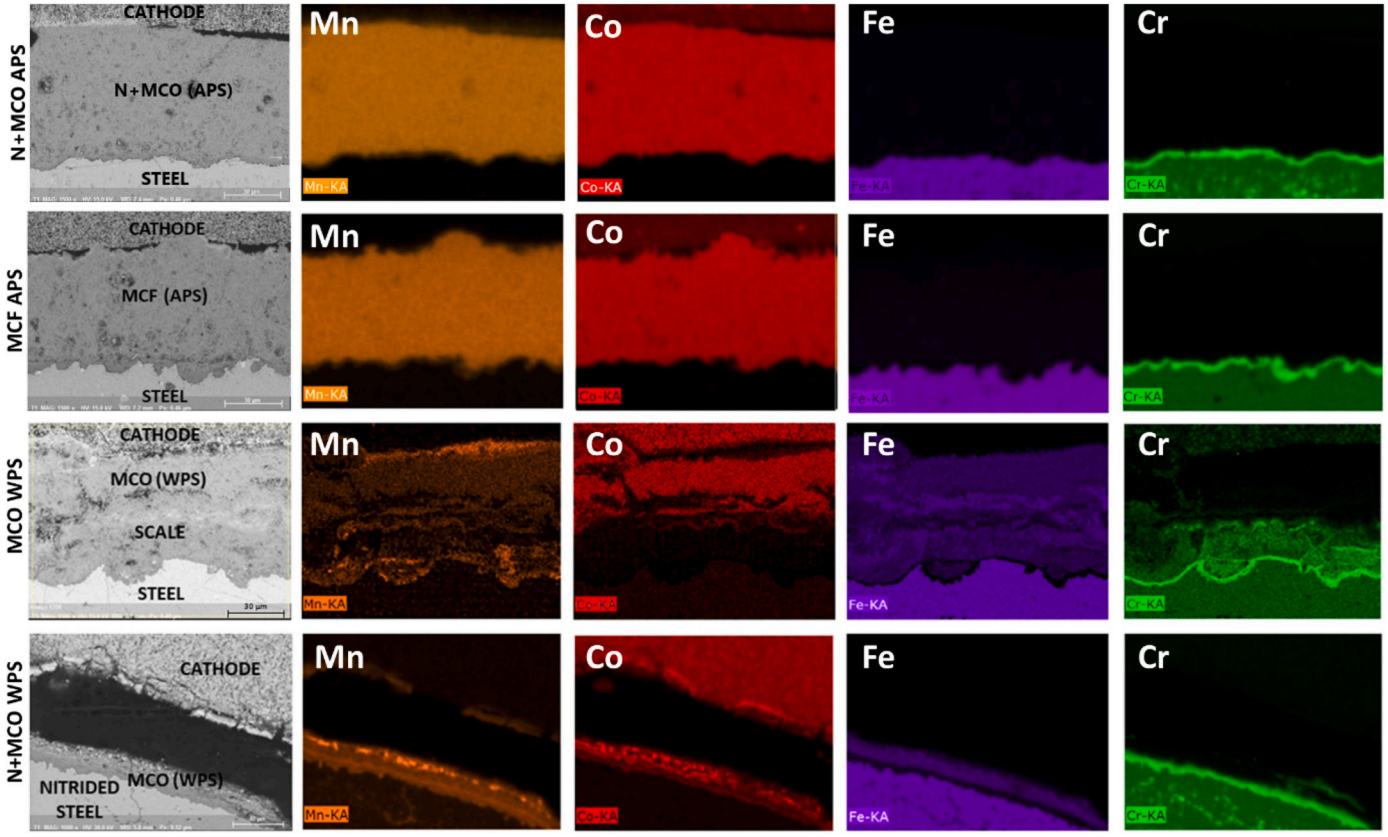

Fig. 2. Comparison of MICs tested for 10 000 h in 6-cell short stack B (Table 2) via MIC/cathode interface cross sections. Starting from the top: MCO deposited via APS on nitrided steel substrate (cell 3 or 5); MCF deposited with APS on standard stainless steel (cell 2 or 4); MCO deposited via WPS on standard steel substrate (cell 1 or 6); WPS-deposited MCO on nitrided substrate (from stack A). (magnification = 1500x).

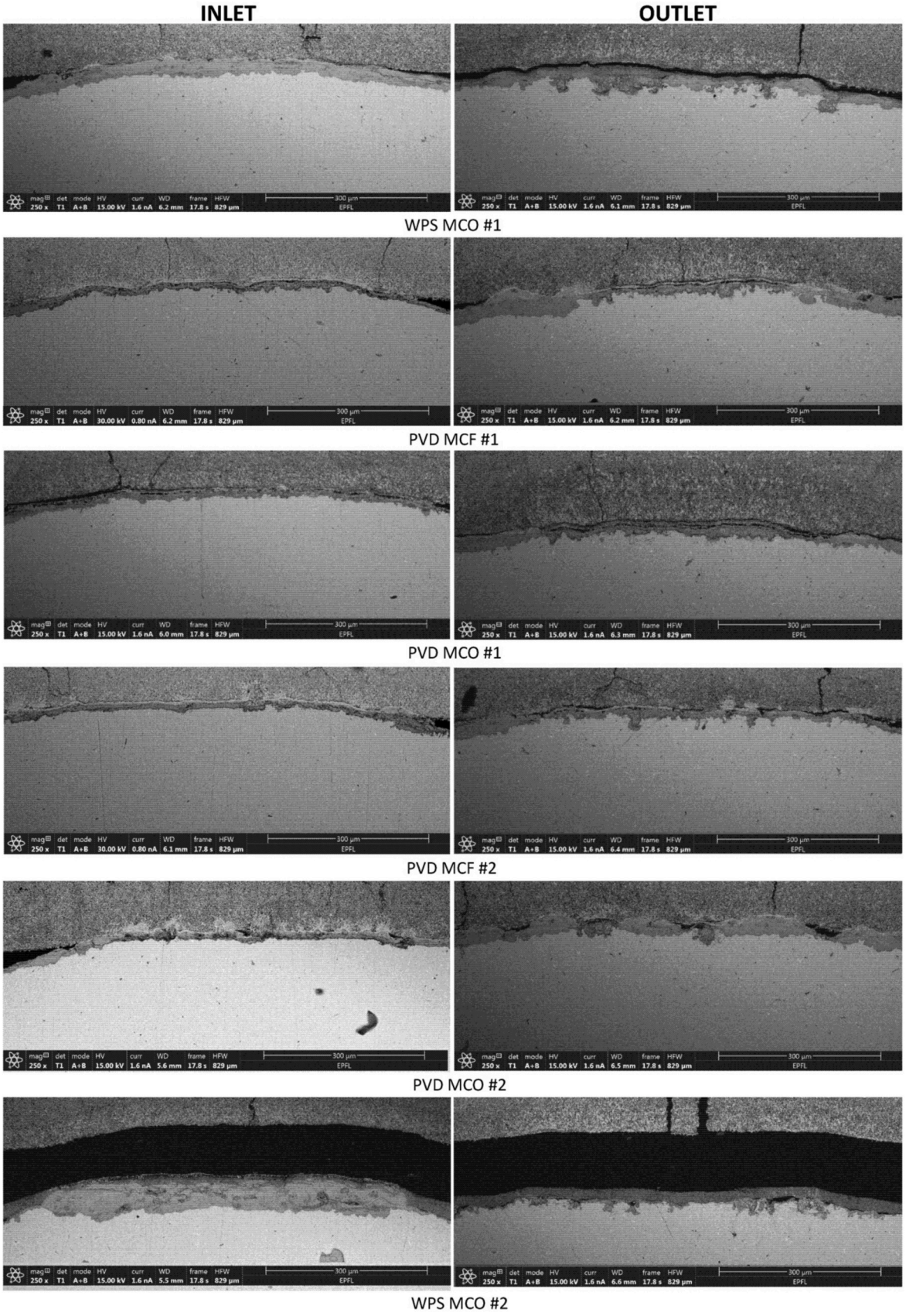

Fig. 3. Comparison of MIC/perovskite interface for all 6 SRUs in stack C at inlet (left column) and outlet (right column). Magnification 250x

PVD-deposited coatings limit the oxidation layer thickness and succeed in stopping chromium migration towards the cathode materials [29]. However, the observations on the stack cross-sections indicate that for PVD-coated MICs tested in a real stack environment, this desired behaviour is present only in a limited portion of the whole MIC/perovskite interface. In other words, looking at this interface in PVD coated MICs, most of the interface will present $SrCrO_4$ or aggravated corrosion (represented by the thick light grey oxidation products).

A different MIC corrosion behaviour is observed between inlet and outlet cross sections. When the interconnects are PVD coated, the aggravated corrosion takes place preferentially at the outlet and $SrCrO_4$ passivation at the inlet; whereas with WPS coated MICs, the behaviour is inverted. Similarly to Cr_2O_3, $SrCrO_4$ passivates the surface because it is thermodynamically stable and decreases the oxidation reaction rate at the steel surface. For the SRUs containing a porous coating (WPS), the transport of strontium vapours at the outlet can explain the different behaviours. Strontium diffuses via the gas phase and the accumulation of chromium vapours could lead to preferred formation of $SrCrO_4$ rather than other corrosion products.

In Fig. 3 the aggravated corrosion regions are thicker, light-grey and the coating is densified. A good example is WPS MCO #2 at the inlet, where above the steel substrate (lightest grey) there is a dense oxide layer of ca. 50 μm. On the other hand, WPS MCO #2 at the outlet is the reference case for strontium chromate formation. The regions with strontium chromate are darker, penetrate into the steel substrate and the coating in presence of $SrCrO_4$ is still porous.

Overall, with WPS coated interconnects, aggravated corrosion similar to iron-breakaway [46] is the most observed degradation process. When this phenomenon takes place, oxygen migrates inwards into the steel substrate, leading to the formation of a hemispheric oxide layer. The EDS analyses of these regions reveal different spinel oxides containing Mn, Co, Fe and Cr. Symmetrically, iron ions migrate from the steel substrate to the coating.

The amount of iron diffused into the coating is not constant, it varies between 20 and 35 at.%. As a result, it is not possible to determine the stoichiometry of the new spinel phases. However, the infiltration of iron is positive in terms of electrical conduction; comparison of the electrical properties of MCF and MCO coated samples demonstrated that the former are performing better [47].

$SrCrO_4$ presence is especially obvious in WPS MCO #2 at the outlet side.

Besides $SrCrO_4$ and outward growth of iron oxides, another undesired reaction product in WPS MCO #2 is a 5 μm thick phase at the MCO/perovskite contact area. The EDS chemical analysis of this zone detected Mn (24 at.%), Sr (21 at.%), Co (4 at.%) and oxygen (51 at.%). It is mostly encountered at the inlet of WPS MCO #1. This stoichiometry, also considering the measurement error, does not clearly point to a compound, as the oxygen is not sufficient for $SrMnO_3$ and other compounds such as $SrMnO_{2.5}$ are unlikely. Above this layer, an accumulation of strontium is found as well. The segregation of strontium from perovskites is a known phenomenon in the SOFC field [48–50]. The presence of a strontium containing oxide is problematic for the stack lifetime because of the low electrical conductivity of some of these compounds [51]. Beside this, a mismatch of coefficient of thermal expansion between $SrCrO_4$ [20] and the cathode materials exists and it can explain the sharp decreases in the voltage values of WPS MCO #2, coincident with an unwanted temperature decrease in the stack.

Regarding the PVD coated interconnects, the dense coating is expected to stop element diffusion, the same way as for the APS coatings in stack B. However, strontium chromate was regularly found below the original PVD coating. In addition, the coating itself presented porosity coalescence. A detailed analysis at high magnification revealed a strontium diffusion path through the PVD coatings, independent of their composition, as displayed in Fig. 4 with PVD MCO #2.

Aggravated corrosion is present in the PVD coated SRUs. This is particularly visible in the PVD MCO #2 outlet cross section (Fig. 3). This interface is interesting because it alternates Fe oxidation areas (wide, smooth, light grey and protruded towards the perovskite) with $SrCrO_4$ ones (narrow, dark grey border, expanding towards the steel substrate).

Close to the regions where the oxides of chromium and strontium are formed in the PVD coated interconnect, there is also a third region where the oxide is the expected SiO_2/Cr_2O_3 only; i.e. the scale composition typically described for the oxidation of this type of ferritic stainless steel. These oxide regions are also thinner than those where the aggravated corrosion takes place; electrical current will therefore choose those preferred pathways.

Referring to the whole Stack C, all six coatings failed in entirely blocking chromium contamination of the perovskite material. This was expected for the WPS coatings but not for PVD. Fig. 4 shows also the migration of chromium from the steel substrate.

3.2. Electrochemical impedance spectroscopy

Fig. 5 presents electrochemical impedance data taken for stack B at different operating times (hours 0, 1000 and 10 000). It confirms that the SRUs containing protective coating APS MCF #1 suffered aggravated degradation similar to WPS MCO #1.

Fig. 6 displays in a more readable representation the ohmic and polarisation losses for the SRUs in stack B. The ohmic resistance values at the beginning of the test were markedly different among the six SRUs, with up to 0.15 (Ohm cm^2) of difference between APS MCF #2 and WPS MCO #1.

After 1000 h of operation, the increase in ohmic losses for all SRUs was modest, generally less than 0.02 Ohm cm^2. Between 1000 and 1 0000 h instead there was a significant increase in the ohmic resistance values, with the maximum increase of 0.24 Ohmcm^2 for APS MCF #1. For this SRU and WPS MCO #1, the ohmic losses accounted for more than 60% of the total resistance.

Excluding APS MCF #1, all APS containing SRUs had a starting value of ohmic resistance around 0.36 Ohm cm^2. The WPS #2 starts with 0.41 Ohm cm^2 and the WPS #1 with 0.51 Ohm cm^2. This difference at the starting point of operation is likely partly related to the temperature distribution: WPS #1 was closer to the bottom of the stack and therefore colder. Thermal losses influence the performances of the 6th repeat unit

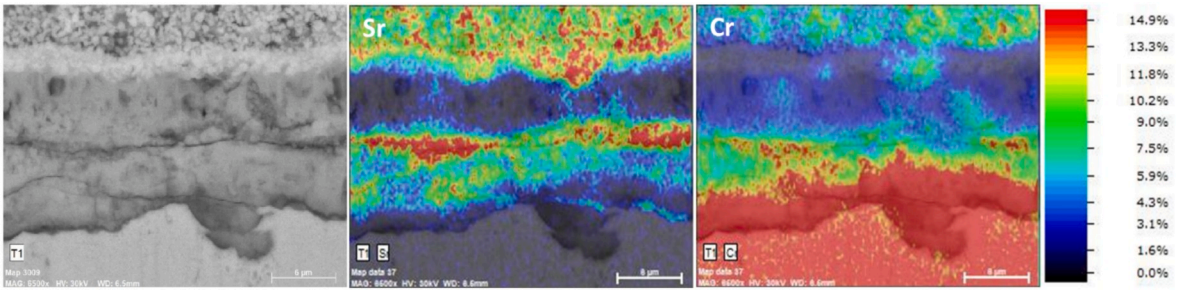

Fig. 4. Quantitative element map of the perovskite/MIC interface for PVD MCO #2, Stack C. Element concentration in at.%.

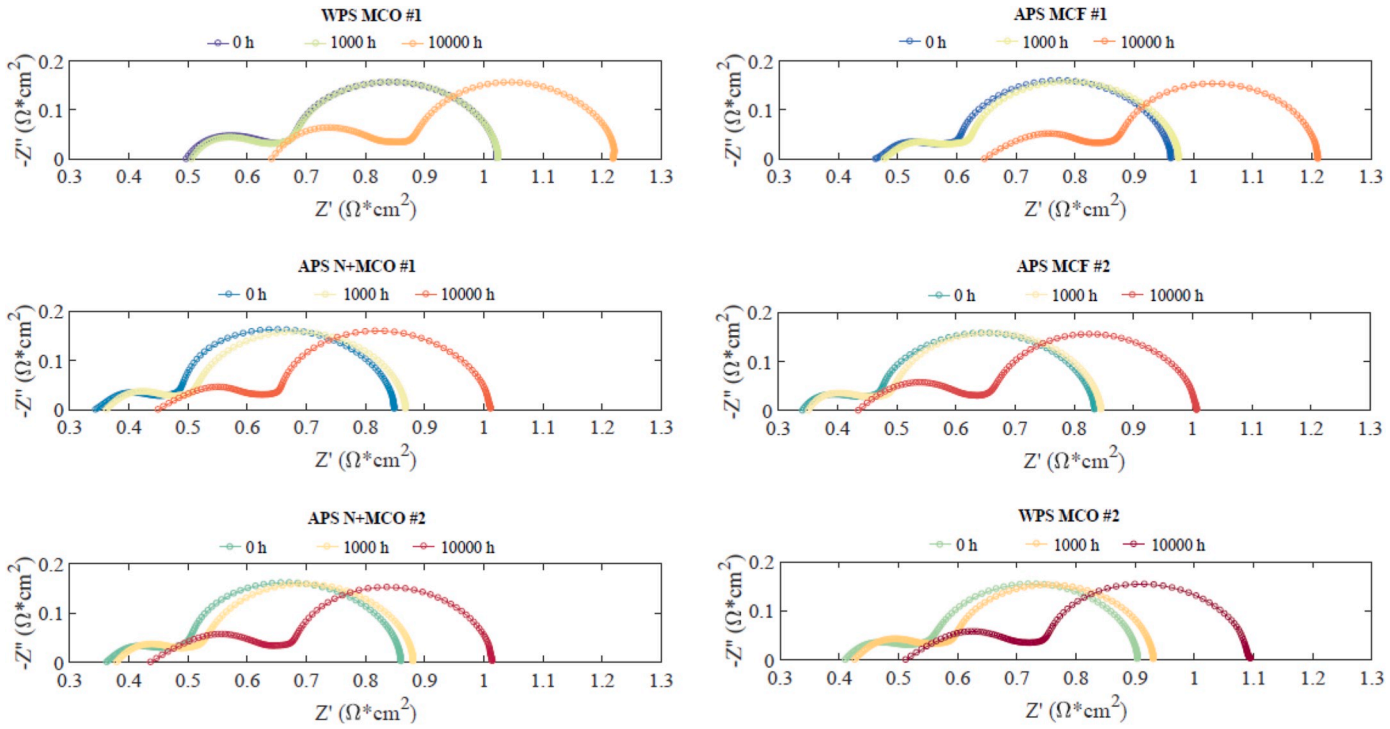

Fig. 5. Electrochemical impedance spectra for Stack B (temperature 750 °C, gas flows air 27 mL/cm^2 fuel 5.5 mL/cm^2, current bias 0.125 A/cm^2, amplitude of perturbation 50 mV, and frequency range 20 kHz to 10 mHz.

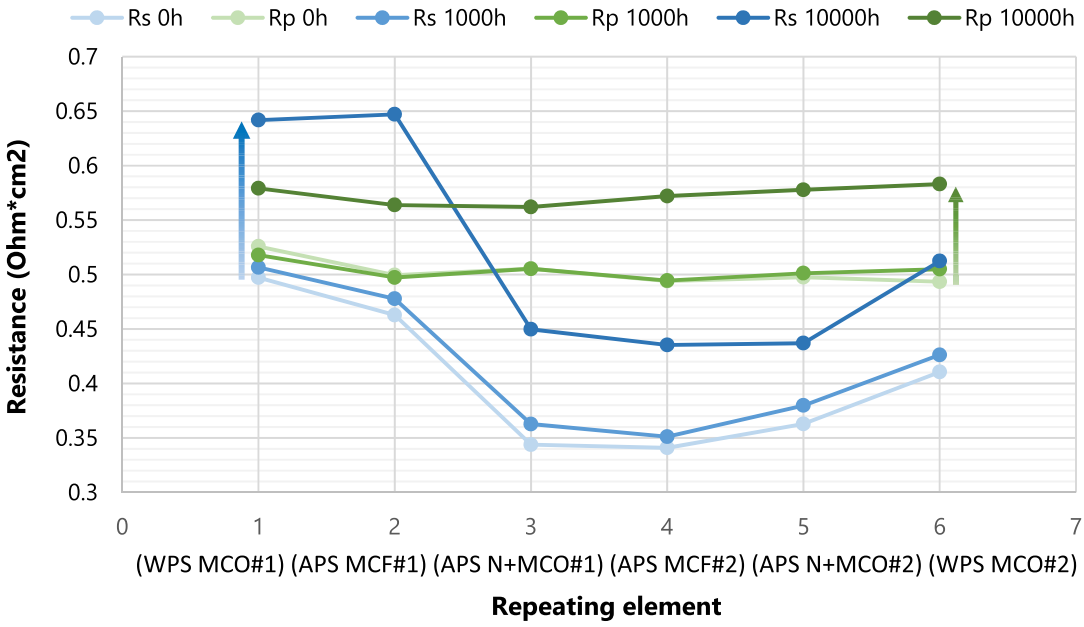

Fig. 6. Representation of the ohmic and polarisation losses for the six SRUs of stack B at 0, 1000 and 10 000 h. Blue lines indicate ohmic type losses. (For interpretation of the references to colour in this figure legend, the reader is referred to the Web version of this article.)

as well, this being partially counterbalanced by the temperature distribution profile, with the temperature higher at the top.

The changes in polarisation losses are similar among the different SRUs, with an increase between 50 and 90 mOhm cm^2. From this data the coatings show no significant influence on the polarisation losses.

The comparison with MICs made of Crofer 22 APU or H steels is unfortunately not possible, as few post-test observations from stacks have been disclosed in literature and the testing conditions are different from those of the stacks presented here [34,35].

The SEM/EDS observations of the APS SRU cross sections did not reveal significant morphological or chemical differences between APS MCF#1 and #2. Also, the cell in the APS MCF#1 does not present any clear defect or contamination It is therefore not possible to determine the cause for the higher degradation value. The presence of a defective

region in a non-observed portion of the stack could be a possibility.

Considering stack C, impedance spectra for the six SRUs were taken at 10 000 h of operation. The Nyquist plot in Fig. 7a displays an anomalous ohmic resistance of the WPS MCO #2 SRU, confirming the high degradation rate shown in Table 2. The EIS measurement conditions are: temperature 750 °C, flows as operation, bias 8 A (0.1 A/cm^2), amplitude 1 A (0.012 in A/cm^2), frequency range 10 kHz–50 kHz.

The investigation of its EI spectrum through the distribution of relaxation times (DRT) is reported in Fig. 7b. The peak P2 (gas conversion) shows the highest peak amplitude for all the SRUs, which is expected since the impedance measurements are acquired with a very small bias current (0.1 A/cm^2 bias) in dry hydrogen condition. Thus, polarisation losses due to gas conversion at these operating conditions are dominant but independent of the electrode performances. Considering the polarisation losses in the middle frequency range (10–1000 Hz), it is clear that the SRU WPS MCO #2 deviates from the others because of higher polarisation losses. Both peaks P3 and P4 register an increase in resistance and a shift towards smaller frequencies. The same behaviour was observed with another stack test where an SRU (the 4th) was purposefully assembled with an insulating material covering 11% of the interconnect contact area (Fig. 7c) [52]). In this figure, the DRT spectra of the two WPS-MCO SRUs (#1 and #2) are compared with the aforementioned stack to look for similarity. The variation of the DRT peaks between the healthy and faulty element of this stack follow the same trend as the WPS MCO SRUs (Fig. 7c) [52].

On the other hand, the remaining spectra revealed no anomalies of the corresponding SRUs. The similarity shift of the peaks in WPS MCO #2 spectrum suggests that the Sr–Mn oxides found at the MIC/perovskite interface has low electrical conductivity such as the insulating material covering the stack [52].

Regarding polarisation losses, the difference in values between the PVD and WPS SRUs is below 0.1 Ohm cm^2, while the difference in ohmic losses is almost 0.3 Ohm cm^2. Moreover, the comparison of impedance spectra of WPS MCO SRUs (Figs. 5 and 7a) taken at different times, up to 10 000 h of operation, indicates a stabilisation over time of the polarisation losses. Hence, ohmic losses are the main responsible for voltage degradation during prolonged operation.

To summarise, merging the information obtained from SEM-EDS

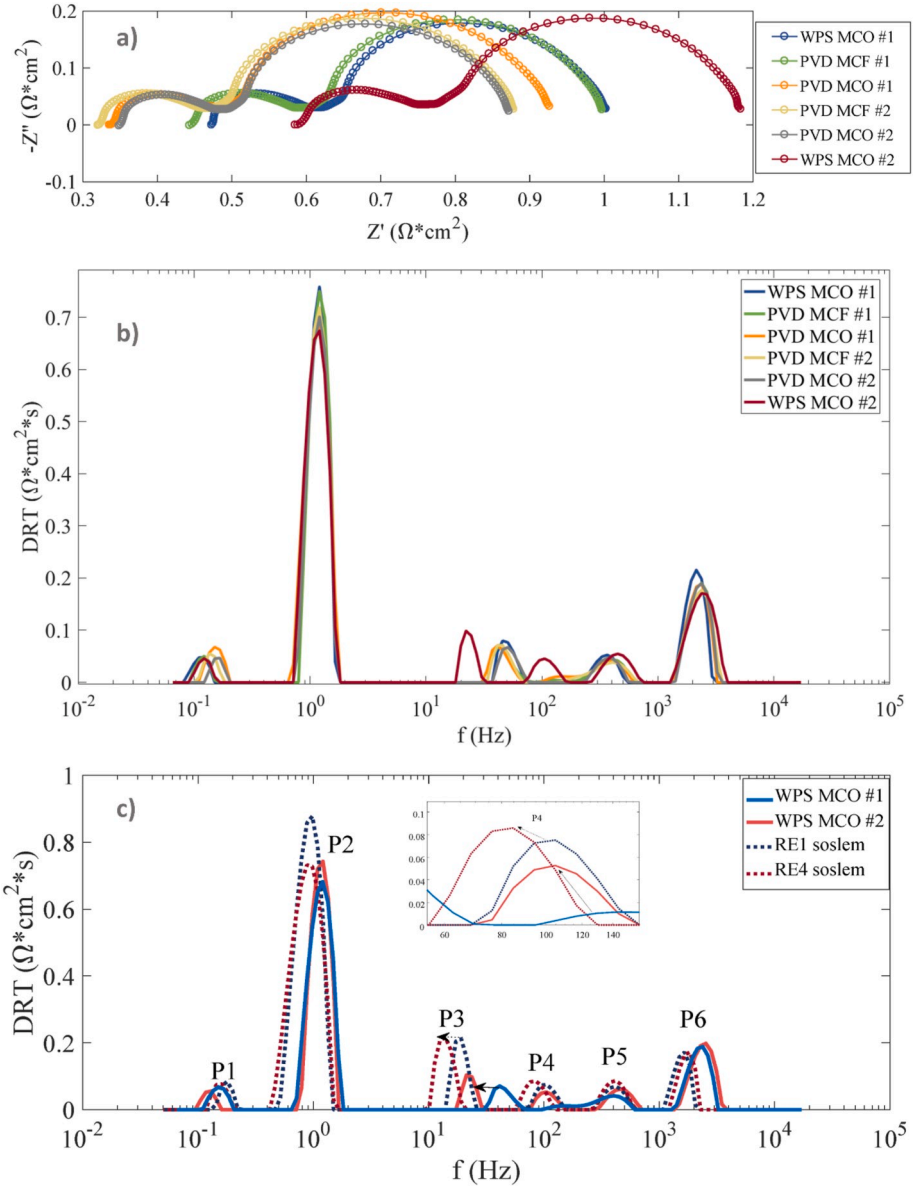

Fig. 7. a) Impedance spectra of the SRUs tested in stack C at 10 000 h. b) Distribution of relaxation times (DRT) treated spectra of the SRUs tested in stack C. c) Comparison of DRT spectra for the WPS MCO SRU in stack C and an SRU with a known contact defect (analysed in a parallel EU project, 'SoSLeM').

analysis with that coming from electrochemical impedance spectroscopy, in presence of a porous WPS coating the ohmic losses and the degradation rate in AISI 441/K41 MICs increase due to: i) the thickening of the oxide layer growing on the interconnect surface, ii) the formation of a low conductive phase, $SrCrO_4$, instead of Cr_2O_3 at the steel/coating interface, and iii) the formation of a Sr containing compound at the MIC/perovskite interface.

These degradation phenomena also took place in the PVD coated SRUs but with slower kinetics. However, the voltage degradation rate for these SRUs is far below the desired threshold of 0.5 $\%kh^{-1}$. A likely explanation is that the presence of contact regions where there is no major corrosion (i.e. no Fe oxidation or $SrCrO_4$ formation) helped the performance of the PVD coated MICs via preferred current paths, thus representing the main reason for the better behaviour of PVD SRUs as compared to WPS SRUs.

APS coated MICs presented satisfactory stability, with a performance degradation between that for WPS and PVD MICs. The thick protective coating (>50 μm) and its hardness, preventing a good contact between the MIC and the perovskite, are the main technical limitations of this deposition method.

3.3. Practical application

40 000 and 80 000 h are, respectively, the minimum and the desired operation lifetimes for SOFC stacks in stationary applications. Considering the empirical values of Table 2, an attempt to predict the voltage values to these lifetimes is performed in Table 3 on 4 cases of interest, assuming a simple linear extrapolation. The degradation performance is sorted lowest to highest as PVD MCO #1 > PVD average > APS average > WPS average. WPS MCO #2 stack C and APS MCF #1 degradation values were not considered in the average as these SRUs showed an anomalous behaviour.

To calculate these values, the voltage of the cells at 1 000 h was taken as a starting point. Then the degradation values of Table 2 are multiplied for 41 000 and 81 000 h, and results were subtracted from the values at 1000 h.

These numbers are only very crudely indicative, but it can nonetheless be inferred that among PVD and APS technology, the former seems preferable. This is interesting because currently APS is preferred over PVD for depositing dense coatings [34].

The MICs represent 10%–30% of the stack cost [5], and, in turn, the raw materials are estimated to account for 40% of the MIC production cost. Initial infrastructure investment is certainly higher for APS and PVD techniques. A complete cost estimation is however not included in this article as it is strongly influenced by the volume production, and the definition of production scenarios is out of the scope of the paper.

4. Conclusion

This study compared different solutions for AISI441/K41 metal interconnects tested in SOFC stack operating conditions and provided information on their behaviour up to 10 000 h. Specifically, single repeating units containing interconnects coated with Mn–Co-based spinels deposited via atmospheric plasma spraying, physical vapour deposition, and wet powder spraying were compared. The cells were identical in all the SRUs; the steel substrate in some cases underwent a surface-nitriding process. The short stack degradation was analysed both at the macroscopic (V(t) curves, EIS analysis) and at the microscopic level (SEM/EDS). The analyses of the results gave new indications for the future choices of MICs and their coatings.

The main findings were:

- Despite its reduced chromium content, AISI441/K41 demonstrated to be a reliable interconnect solution in SOFC stacks over extended test time if coated appropriately. Its degradation was influenced mainly by the coating deposition technique.

Table 3
Average voltage values (Volts) extrapolated for four types of SRU.

	PVD MCO #1	PVD average	APS average	WPS average
40000 h	0.764	0.717	0.624	0.562
80000 h	0.75	0.668	0.477	0.388

- Nitriding of the steel substrates helped the chromium retention properties in case of porous coatings. The diffused chromium measured in the perovskite contact layer for the case of nitrided SRUs was similar to that of (dense) APS-coated SRUs.
- APS-coating confirmed excellent chromium retention properties, independently of the coating composition. However, the SRUs containing MICs coated with APS showed a faster degradation compared to PVD-coated SRUs. The hardness and the thickness of the coating were suspected to be the main responsible sources for higher ohmic losses.
- Single repeating units containing PVD coatings showed the lowest degradation rates, despite the presence of non-uniform corrosion processes: aggravated corrosion (outward growth of iron oxides and inwards oxidation of the steel substrate), similar to iron breakaway corrosion, and strontium chromate are found after SEM investigations.
- A forecasting of the voltage degradation for 40 000 and 80 000 h of operation assuming linear extrapolation indicates PVD-containing SRUs as the preferable ones, followed by APS and finally WPS.
- Results derived from small samples [29] were not always confirmed by results on short stacks (this study).

Declaration of competing interest

The authors declare that they have no known competing financial interests or personal relationships that could have appeared to influence the work reported in this paper.

CRediT authorship contribution statement

Manuel Bianco: Conceptualization, Data curation, Formal analysis, Investigation, Methodology, Software, Validation, Visualization, Writing - original draft. **Priscilla Caliandro:** Data curation, Formal analysis, Investigation, Methodology, Software, Writing - review & editing. **Stefan Diethelm:** Investigation, Writing - review & editing, Supervision. **Shicai Yang:** Formal analysis, Resources, Writing - review & editing. **Alessandro Dellai:** Formal analysis, Resources, Writing - review & editing. **Jan Van herle:** Writing - review & editing, Supervision. **Robert Steinberger-Wilckens:** Conceptualization, Funding acquisition, Project administration, Supervision, Writing - review & editing.

Acknowledgements

The authors thank all partners in the project SCoReD 2:0 for their contributions to the results presented in this paper, and especially Francesco Bozza for applying the APS coatings.

The research leading to these results received funding from the European Union's Seventh Framework Programme (FP7/2007-2013) through the Fuel Cells and Hydrogen Joint Undertaking under grant agreement no. 325331 for project SCoReD 2:0. Swiss partners are funded from the Swiss State Secretariate for Education, Research and Innovation SEFRI under contract 16.0042.

Appendix A. Supplementary data

Supplementary data to this article can be found online at https://doi.org/10.1016/j.jpowsour.2020.228163.

References

[1] N.H. Menzler, D. Sebold, O. Guillon, Post-test characterization of a solid oxide fuel cell stack operated for more than 30,000 hours: the cell, J. Power Sources 374 (2018) 69–76, https://doi.org/10.1016/j.jpowsour.2017.11.025.

[2] M. Bertoldi, O. Bucheli, A. Ravagni, Development, manufacturing and deployment of SOFC-based products at SOLIDpower, ECS Trans 78 (2017) 117–123.

[3] F. Baldi, L. Wang, M. Pérez-Fortes, F. Maréchal, A cogeneration system based on solid oxide and proton exchange membrane fuel cells with hybrid storage for off-grid applications, Front. Energy Res. 6 (2019), https://doi.org/10.3389/fenrg.2018.00139.

[4] J. Wu, X. Liu, Recent development of SOFC metallic interconnect, J. Mater. Sci. Technol. 26 (2010) 293–305, https://doi.org/10.1016/S1005-0302(10)60049-7.

[5] J.W. Fergus, Synergism in the design of interconnect alloy–coating combinations solid for oxide fuel cells, Scripta Mater. 65 (2011) 73–77, https://doi.org/10.1016/j.scriptamat.2010.09.020.

[6] N.K. Othman, J. Zhang, D.J. Young, Water vapour effects on Fe–Cr alloy oxidation, Oxid. Metals 73 (2010) 337–352, https://doi.org/10.1007/s11085-009-9183-9.

[7] Z. Yang, G. Xia, P. Singh, J.W. Stevenson, Effects of water vapor on oxidation behavior of ferritic stainless steels under solid oxide fuel cell interconnect exposure conditions, Solid State Ionics 176 (2005) 1495–1503, https://doi.org/10.1016/j.ssi.2005.03.019.

[8] M.S. Khan, S.-B. Lee, R.-H. Song, J.-W. Lee, T.-H. Lim, S.-J. Park, Fundamental mechanisms involved in the degradation of nickel–yttria stabilized zirconia (Ni–YSZ) anode during solid oxide fuel cells operation: a review, Ceram. Int. 42 (2016) 35–48, https://doi.org/10.1016/j.ceramint.2015.09.006.

[9] M. Rafique, H. Nawaz, M.S. Rafique, M.B. Tahir, G. Nabi, N.R. Khalid, Material and method selection for efficient solid oxide fuel cell anode: recent advancements and reviews, Int. J. Energy Res. 43 (2019) 2423–2446, https://doi.org/10.1002/er.4210.

[10] J.H. Zhu, H. Ghezel-Ayagh, Cathode-side electrical contact and contact materials for solid oxide fuel cell stacking: a review, Int. J. Hydrogen Energy 42 (2017) 24278–24300, https://doi.org/10.1016/j.ijhydene.2017.08.005.

[11] F.S. da Silva, T.M. de Souza, Novel materials for solid oxide fuel cell technologies: a literature review, Int. J. Hydrogen Energy 42 (2017) 26020–26036, https://doi.org/10.1016/j.ijhydene.2017.08.105.

[12] S. Poitel, Y. Antonnetti, Z. Wuillemin, J. Van herel, C. Hébert, The effect of polarization on SOFC seal ageing, XII EFCF Proc B05 (2016) 88–97.

[13] M. Rautanen, V. Pulkkinen, J. Tallgren, O. Himanen, J. Kiviaho, Effects of the first heat up procedure on mechanical properties of solid oxide fuel cell sealing materials, J. Power Sources 284 (2015) 511–516, https://doi.org/10.1016/j.jpowsour.2015.03.012.

[14] J.-H. Hsu, C.-W. Kim, R.K. Brow, J. Szabo, R. Crouch, R. Baird, An alkali-free barium borosilicate viscous sealing glass for solid oxide fuel cells, J. Power Sources 270 (2014) 14–20, https://doi.org/10.1016/j.jpowsour.2014.07.088.

[15] S.J. McPhail, D. Pumiglia, J. Laurencin, A. Hagen, A. Leon, J.V. Herle, D. Vladikova, D. Montinaro, P. Piccardo, P. Polverino, K. Herbrig, Developing accelerated stress test protocols for solid oxide fuel cells and electrolysers: the European project AD ASTRA, ECS Trans 91 (2019) 563, https://doi.org/10.1149/09101.0563ecst.

[16] L. Blum, Q. Fang, S.M. Groß-Barsnick, L.G.J.(Bert, de Haart, J. Malzbender, N. H. Menzler, W.J. Quadakkers, Long-term operation of solid oxide fuel cells and preliminary findings on accelerated testing, Int. J. Hydrogen Energy 45 (2020) 8955–8964, https://doi.org/10.1016/j.ijhydene.2020.01.074.

[17] A. Ploner, A. Hagen, A. Hauch, Classical statistical methodology for accelerated testing of solid oxide fuel cells, J. Power Sources 395 (2018) 379–385, https://doi.org/10.1016/j.jpowsour.2018.05.034.

[18] W.J. Quadakkers, J. Piron-Abellan, V. Shemet, L. Singheiser, Metallic interconnectors for solid oxide fuel cells – a review, Mater. A. T. High. Temp. 20 (2003) 115–127, https://doi.org/10.1179/mht.2003.015.

[19] J.A. Schuler, C. Gehrig, Z. Wuillemin, A.J. Schuler, J. Wochele, C. Ludwig, A. Hessler-Wyser, J. Van herle, Air side contamination in solid oxide fuel cell stack testing, J. Power Sources 196 (2011) 7225–7231, https://doi.org/10.1016/j.jpowsour.2010.10.058.

[20] T. Zhang, R.K. Brow, W.G. Fahrenholtz, S.T. Reis, Chromate formation at the interface between a solid oxide fuel cell sealing glass and interconnect alloy, J. Power Sources 205 (2012) 301–306, https://doi.org/10.1016/j.jpowsour.2012.01.043.

[21] M.R. Ardigò, A. Perron, L. Combemale, O. Heintz, G. Caboche, S. Chevalier, Interface reactivity study between La0.6Sr0.4Co0.2Fe0.8O3−δ (LSCF) cathode material and metallic interconnect for fuel cell, J. Power Sources 196 (2011) 2037–2045, https://doi.org/10.1016/j.jpowsour.2010.09.063.

[22] K. Fujita, T. Hashimoto, K. Ogasawara, H. Kameda, Y. Matsuzaki, T. Sakurai, Relationship between electrochemical properties of SOFC cathode and composition of oxide layer formed on metallic interconnects, J. Power Sources 131 (2004) 270–277, https://doi.org/10.1016/j.jpowsour.2003.12.050.

[23] P. Tanasini, C. Comninellis, J. Van herle, Modelling-Assisted Investigation of Degradation Phenomena in LSM-Based SOFC Composite Cathodes, EPFL, 2011. https://infoscience.epfl.ch/record/163534.

[24] H. Yokokawa, T. Horita, K. Yamaji, H. Kishimoto, T. Yamamoto, M. Yoshikawa, Y. Mugikura, K. Tomida, Chromium poisoning of LaMnO3-based cathode within generalized approach, Fuel Cell. 13 (2013) 526–535, https://doi.org/10.1002/fuce.201200164.

[25] S.P. Jiang, X. Chen, Chromium deposition and poisoning of cathodes of solid oxide fuel cells – a review, Int. J. Hydrogen Energy 39 (2014) 505–531, https://doi.org/10.1016/j.ijhydene.2013.10.042.

[26] J.C.W. Mah, A. Muchtar, M.R. Somalu, M.J. Ghazali, Metallic interconnects for solid oxide fuel cell: a review on protective coating and deposition techniques, Int. J. Hydrogen Energy 42 (2017) 9219–9229, https://doi.org/10.1016/j.ijhydene.2016.03.195.

[27] N. Shaigan, W. Qu, D.G. Ivey, W. Chen, A review of recent progress in coatings, surface modifications and alloy developments for solid oxide fuel cell ferritic stainless steel interconnects, J. Power Sources 195 (2010) 1529–1542, https://doi.org/10.1016/j.jpowsour.2009.09.069.

[28] Y. Larring, T. Norby, Spinel and perovskite functional layers between plansee metallic interconnect (Cr-5 wt % Fe-1 wt % Y 2 O 3) and ceramic (La0.85Sr0.15) 0.91MnO3 cathode materials for solid oxide fuel cells, J. Electrochem. Soc. 147 (2000) 3251–3256, https://doi.org/10.1149/1.1393891.

[29] M. Bianco, J. Tallgren, J.-E. Hong, S. Yang, O. Himanen, J. Mikkola, J. Van herle, R. Steinberger-Wilckens, Ex-situ experimental benchmarking of solid oxide fuel cell metal interconnects, J. Power Sources 437 (2019), 226900, https://doi.org/10.1016/j.jpowsour.2019.226900.

[30] J. Tallgren, M. Bianco, O. Himanen, O. Thomann, J. Kiviaho, J. van Herle, Evaluation of protective coatings for SOFC interconnects, ECS Trans 68 (2015) 1597–1608, https://doi.org/10.1149/06801.1597ecst.

[31] S. Frangini, A. Masi, L.D. Seta, M. Bianco, J.V. Herle, Composite Cu-LaFeO3 conversion coatings on a 18Cr ferritic stainless steel for IT-SOFC interconnects: effect of long-term air exposure at 700°C on Cr diffusion barrier and electrical properties, J. Electrochem. Soc. 165 (2018) F97–F104, https://doi.org/10.1149/2.0101803jes.

[32] V.D.M. Metals, Crofer 22 H Material Data Sheet, VDM Metals, 2010.

[33] K41 technical data sheet, ArcelorMittal, n.d, http://www.aperam.com/uploads/stainlesseurope/TechnicalDataSheet/FT_K41X_Eng.pdf. accessed November 15, 2017.

[34] N.H. Menzler, P. Batfalsky, A. Beez, L. Blum, S. Gross-Barsnick, L. Niewolak, Post-test analysis of a solid oxide fuel cell stack operated for 35,000 h, XII EFCF proceedings A11 (2016) 290–297.

[35] N.H. Menzler, P. Batfalsky, S. Groß, V. Shemet, F. Tietz, Post-test characterization of an SOFC short-stack after 17,000 hours of steady operation, ECS Trans 35 (2011) 195–206, https://doi.org/10.1149/1.3569994.

[36] J. Malzbender, P. Batfalsky, R. Vaßen, V. Shemet, F. Tietz, Component interactions after long-term operation of an SOFC stack with LSM cathode, J. Power Sources 201 (2012) 196–203, https://doi.org/10.1016/j.jpowsour.2011.10.117.

[37] Q. Fang, L. Blum, P. Batfalsky, N.H. Menzler, U. Packbier, D. Stolten, Durability test and degradation behavior of a 2.5 kW SOFC stack with internal reforming of LNG, Int. J. Hydrogen Energy 38 (2013) 16344–16353, https://doi.org/10.1016/j.ijhydene.2013.09.140.

[38] S.M. Groß-Barsnick, Q. Fang, P. Batfalsky, L. Niewolak, L. Blum, W.J. Quadakkers, Post-test characterization of metallic materials and adjacent components in an SOFC stack after 34,000 h operation at 700 °C, Fuel Cell. 19 (2019) 84–95, https://doi.org/10.1002/fuce.201800050.

[39] M. Bianco, M. Linder, Y. Larring, F. Greco, J. Van herle, Lifetime issues for solid oxide fuel cell interconnects, in: N. Brandon (Ed.), Solid Oxide Fuel Cell Lifetime Reliab, ELSEVIER, the Netherlands, 2017.

[40] R. Scataglini, M. Wei, A. Mayyas, S.H. Chan, T. Lipman, M. Santarelli, A direct manufacturing cost model for solid-oxide fuel cell stacks, Fuel Cell. 17 (2017) 825–842, https://doi.org/10.1002/fuce.201700012.

[41] Manufacturing Cost Analysis of 1 kW and 5 kW Solid Oxide Fuel Cell (SOFC) for Auxilliary Power Applications, BATTELLE, Battelle Memorial Institute 505 King Avenue Columbus, 2014. OH 43201, https://energy.gov/sites/prod/files/2014/06/f16/fcto_battelle_cost_analysis_apu_feb2014.pdf. accessed February 10, 2017.

[42] S. Harboe, A. Schreiber, N. Margaritis, L. Blum, O. Guillon, N.H. Menzler, Manufacturing cost model for planar 5 kWel SOFC stacks at Forschungszentrum Jülich, Int. J. Hydrogen Energy 45 (2020) 8015–8030, https://doi.org/10.1016/j.ijhydene.2020.01.082.

[43] H. Yokokawa, T. Horita, N. Sakai, K. Yamaji, M.E. Brito, Y.-P. Xiong, H. Kishimoto, Thermodynamic considerations on Cr poisoning in SOFC cathodes, Solid State Ionics 177 (2006) 3193–3198, https://doi.org/10.1016/j.ssi.2006.07.055.

[44] T. Gheno, D. Monceau, D.J. Young, Mechanism of breakaway oxidation of Fe–Cr and Fe–Cr–Ni alloys in dry and wet carbon dioxide, Corrosion Sci. 64 (2012) 222–233, https://doi.org/10.1016/j.corsci.2012.07.024.

[45] M. Bianco, S. Poitel, J.-E. Hong, S. Yang, Z.-J. Wang, M. Willinger, R. Steinberger-Wilckens, J. Van herle, Corrosion behaviour of nitrided ferritic stainless steels for use in solid oxide fuel cell devices, Corrosion Sci. (2020), 108414, https://doi.org/10.1016/j.corsci.2019.108414.

[46] F. Abe, H. Araki, H. Yoshida, M. Okada, R. Watanabe, The effect of grain size on the corrosion behaviour of inconel 600 in high-temperature steam, Corrosion Sci. 21 (1981) 819–842, https://doi.org/10.1016/0010-938X(81)90024-X.

[47] J. Tallgren, M. Bianco, J. Mikkola, O. Himanen, M. Rautanen, J. Kiviaho, J. Van herle, Comparison of different manganese-cobalt-iron spinel protective coating for SOFC interconnects, in: XII European SOFC & SOE Forum, 2016, pp. 114–124.
[48] S.P. Simner, M.D. Anderson, M.H. Engelhard, J.W. Stevenson, Degradation mechanisms of La – Sr – Co – Fe – O3 SOFC cathodes, Electrochem. Solid State Lett. 9 (2006) A478–A481, https://doi.org/10.1149/1.2266160.
[49] J.N. Davis, K.F. Ludwig, K.E. Smith, J.C. Woicik, S. Gopalan, U.B. Pal, S.N. Basu, Surface segregation in lanthanum strontium manganite thin films and its potential effect on the oxygen reduction reaction, J. Electrochem. Soc. 164 (2017) F3091–F3096, https://doi.org/10.1149/2.0131710jes.
[50] Y. Yu, K.F. Ludwig, J.C. Woicik, S. Gopalan, U.B. Pal, T.C. Kaspar, S.N. Basu, Effect of Sr content and strain on Sr surface segregation of La1–xSrxCo0.2Fe0.8O3−δ as cathode material for solid oxide fuel cells, ACS Appl. Mater. Interfaces 8 (2016) 26704–26711, https://doi.org/10.1021/acsami.6b07118.
[51] W.D. Copeland, R.A. Swalin, Studies on the defect structure of strontium oxide, J. Phys. Chem. Solid. 29 (1968) 313–325, https://doi.org/10.1016/0022-3697(68)90076-0.
[52] P. Caliandro, Identification of Solid Oxide Cell Elementary Processes by Electrochemical Impedence Spectroscopy, EPFL, 2018.